SINERGI Vol. 30, No. 1, February 2026: 299-318
http://publikasi.mercubuana.ac.id/index.php/sinergi
http://doi.org/10.22441/sinergi.2026.1.027

Overestimation of load-resisting capacity in double-span welded steel beams: a comparative FEM study incorporating ductile damage and element deletion

Nor Idahyu Mohd Zaman, Nur Ezzaryn Asnawi Subki, Yazmin Sahol Hamid, Hazrina Mansor*
Faculty of Civil Engineering, Universiti Teknologi MARA (UiTM) Shah Alam, Malaysia

Abstract
The study investigates how different finite element modelling assumptions affect the predicted load-resisting behavior of welded beam-column connections in double-span steel beam systems subjected to column-removal scenarios. Existing numerical studies commonly neglect fracture and material degradation, which may result in unconservative estimates of structural capacity. To address this limitation, nonlinear static analyses were performed in ABAQUS using two simplified modelling approaches: (i) non-fracture models that exclude plasticity damage and element deletion, and (ii) fracture-based models that incorporate ductile damage criteria with element deletion. Structural responses were evaluated in terms of load-displacement relationships, moment-rotation behavior, and the development of tensile catenary action. The results indicate that accounting for plasticity damage and fracture significantly alters the predicted response, leading to markedly lower strength and deformation capacity compared to non-fracture models. In particular, the inclusion of fracture mechanisms resulted in an approximate 50% reduction in load-carrying capacity and catenary resistance. These findings demonstrate that neglecting fracture behavior can substantially overestimate the robustness of welded beam-column connections under extreme loading conditions. The study underscores the importance of structural performance in progressive collapse analyses.

This is an open-access article under the CC BY-SA license

Keywords:
Element deletion;
Load-displacement curve;
Moment-rotation response;
Numerical simulation;
Plasticity damage;
Tensile catenary action;

Article History:
Received: October 28, 2025
Revised: December 11, 2025
Accepted: December 26, 2025
Published: January 18, 2026

Corresponding Author:
Hazrina Mansor
Faculty of Civil Engineering,
Universiti Teknologi MARA
(UiTM) Shah Alam, Malaysia
Email:
hazrina4476@uitm.edu.my

INTRODUCTION

Steel connections are vital components ensuring the robustness, safety, and efficiency of steel frameworks. They play a crucial role in stabilizing structures, distributing loads effectively between elements like beams and columns, and enhancing overall performance against gravity, wind, seismic activity, and dynamic loads. These connections also promote uniform load distribution, preventing stress concentration points. Moreover, they provide redundancy, ensuring structural stability even if one connection fails. This resilience enhances the reliability of steel structures, enabling them to withstand challenging conditions such as progressive collapse, column removal, or seismic disturbances.

Recent studies increasingly recognize steel beam-to-column connections as critical contributors to structural robustness under extreme events, particularly progressive collapse. Beyond their conventional load-transfer role, connections govern the activation of alternate load paths following local failures, directly influencing system-level stability. The pioneering studies by Yang and Tan demonstrated that bolted connections can effectively sustain catenary action when adequate ductility and tensile capacity are provided [1][2]. Their experimental and numerical investigations

highlighted that connection detailing plays a decisive role in deformation capacity and failure mode once flexural resistance is exhausted. However, these studies were largely confined to specific bolted configurations and isolated sub-assemblages, limiting their broader applicability. Advances in numerical modelling have enabled deeper insight into connection behavior under column removal scenarios. Xie et al. examined fully welded beam-to-column connections and showed that while such joints exhibit high initial stiffness, their ability to accommodate large deformations is constrained by welding details and material nonlinearity, potentially leading to brittle failure [3]. The exclusive focus on welded connections, however, reduces relevance for structures employing bolted or hybrid systems.

Complementary work done by Wang et al. [4] confirmed that connection configuration significantly affects the transition from flexural to catenary action and, consequently, progressive collapse resistance. Despite these contributions, existing studies primarily assess conventional connection forms and do not systematically address optimized designs that balance strength, ductility, and constructability. The literature establishes that connection performance is central to maintaining structural integrity under column loss. Nevertheless, a clear research gap remains in developing optimized steel connection systems through integrated experimental and numerical approaches to enhance robustness across diverse structural applications.

In the scenario of column removal as illustrated in Figure 1, displacement arises due to the external load acting on the column section. As the column is removed, there is a shift in load-distribution, resulting in an increase in loads on adjacent structural elements. The loads that were originally supported by the removed column need to be redistributed among the remaining elements. Consequently, adjacent members that were initially under compression experience an increase in tensile forces to accommodate the additional loads [5]. The redistribution of loads creates an imbalance, causing adjacent elements to develop tensile forces, particularly those that were initially in compression. As the loads are redistributed, some members begin to experience tensile forces. This phenomenon is especially notable for elements initially under compression. As the beams rotate, forces accumulate, eventually leading to connection rupture and failure at a specific rotation angle.

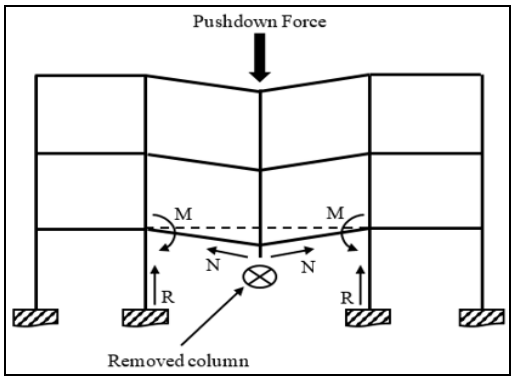

Figure 1. Load-resisting mechanisms in a structure under column removal scenario

However, the complexities of steel connection failure under extreme loading conditions have driven increasing reliance on three-dimensional finite element (FE) modelling to capture detailed geometric, material, and contact nonlinearities. Unlike simplified analytical models, 3D FE analysis enables explicit representation of load transfer mechanisms, damage initiation, and post-elastic behavior, making it particularly suitable for investigating progressive collapse resistance. For bolted steel connections, prior studies have largely adopted modelling simplifications to balance accuracy and computational efficiency. Investigations by Dinu et al., Yang and Tan, Gao, and Ye et al. demonstrated that FE models can effectively reproduce global load-deformation responses even when bolt threads are omitted [1, 6, 7, 8]. This assumption shifts the fidelity of the model toward global structural behavior at the expense of localized stress concentration and slip mechanisms. More critically, the treatment of bolt pretension has emerged as a key source of discrepancy among studies. While Gao [7] and Ye et al. [8] showed that the pretension significantly influences initial stiffness and deformation response, its omission in earlier work by Yang and Tan [1] introduces uncertainty in simulating realistic connection behavior under catenary action.

In contrast, FE modelling of welded connections has pursued higher geometric and material fidelity. Studies by Sulaiman et al. [9] and Zhao et al. [10] employed detailed ply-by-ply and weld bead representations to capture localized plasticity and fracture behavior in butt and T-joints. Complementary investigations by Anca et al. [11] and Wang et al. [4] further highlighted the sensitivity of welded connection performance to weld thickness and thermal effects. Nevertheless, such high-resolution models significantly increase computational cost and often encounter convergence difficulties due

to complex heat flux and thermal-mechanical coupling, particularly in ABAQUS. Existing FE studies reveal a clear trade-off between modelling fidelity and computational feasibility. While simplified approaches enable parametric investigation at the structural level, detailed models offer deeper insight into local failure mechanisms. Bridging this gap remains a critical challenge for developing reliable and efficient predictive frameworks for steel connection behavior under extreme loading conditions.

Conservative finite element modelling of steel connections frequently relies on simplified representations to reduce computational demand while capturing global structural response. One widely adopted strategy is the use of discrete spring or connector elements to idealize bolted connections. Sutherland [12] demonstrated that nonlinear spring models, defined as rigid in compression, can effectively simulate contact behavior in beam-column joints with multiple bolts and continuity plates. This approach enables efficient evaluation of connection stiffness and force transfer mechanisms at the system level. Similar connector-based modelling strategies were adopted by Ye et al. [8], conforming to their suitability for structural-scale analyses. Despite their efficiency, spring-based models introduce a critical dependency on calibration parameters, which are often derived from experimental data. This reliance limits their broader applicability, as acquiring reliable test-based inputs is both time-consuming and costly. Moreover, such models inherently suppress localized stress development and damage evolution, thereby constraining their ability to predict failure mechanisms under extreme loading conditions.

For welded connections, many studies adopt an even more simplified approach by modelling welds using tie constraints, as employed in [6, 13, 14]. While this technique significantly reduces modelling complexity, it implicitly assumes perfect load transfer without degradation, effectively eliminating the possibility of weld fracture or local plasticity. Consequently, tie-based modelling is primarily suitable for scenarios where damage is not expected, such as under service-level or moderately nonlinear loading, consistent with observations in [15, 16, 17]. However, the limitations of these simplified approaches become pronounced when connections are subjected to large deformations or extreme events. In such cases, simplified models may overestimate stiffness and load-carrying capacity, leading to unconservative predictions of structural performance. Therefore, existing literature highlights a fundamental trade-off between computational efficiency and physical realism, underscoring the need for nonlinear behaviors of steel connections.

Advanced finite element modeling of steel connections has increasingly focused on fracture simulation to overcome the inherent limitations of simplified approaches when structural components are subjected to extreme loading. Fracture modelling, as demonstrated by Dinu et al. [6] and Yang and Tan [1], commonly combines progressive ductile damage material models with element deletion techniques. This framework enables explicit simulation of fracture initiation, crack propagation, and ultimate separation by enforcing failure criteria linked to stress triaxiality, plastic strain, or energy dissipation. Compared to simplified models, such approaches provide a more physically realistic representation of connection behavior, particularly in scenarios where fracture governs collapse mechanisms such as catenary action or fire-induced failure. Despite these advantages, the adoption of fracture-based modelling remains limited due to its substantial demands on data quality, computational cost and user expertise. Accurate implementation requires reliable material parameters calibrated against experimental results, as well as careful numerical control to ensure convergence and mesh objectivity. As highlighted in [18, 19, 20], deficiencies in experimental calibration or inappropriate damage parameters can significantly distort predicted failure modes, undermining confidence in the results. Consequently, while fracture modelling offers superior fidelity, its practicality for routine or parametric studies remains constrained.

The consequences of omitting explicit fracture representation are evident in several studies employing simplified modelling techniques. Dai et al. [15], for instance, used simplified numerical models to simulate welded beam-to-column connections subjected to fire loading. Although their finite element analysis captured global structure response, it failed to reproduce the weld fracture observed experimentally in fin plate joints, as the weld was not explicitly modelled. This discrepancy illustrates a fundamental limitation of simplified approaches when local failure mechanisms dominate structural response; models that assume intact connections may yield incomplete or misleading predictions. Similar shortcomings were identified by Liao et al. [16] in their investigation of high-strength steel welded cruciform connections under seismic loading. Using simplified finite element models, they observed that numerical simulations continued to

predict increasing load capacity even after fracture had occurred in physical tests. The divergence between finite element-derived and experimental load-deformation responses following fracture underscores a systematic overestimation of post-peak capacity when damage evolution is neglected. Such discrepancies raise critical concerns regarding the reliability of simplified finite element models for assessing connection performance beyond initial yielding. These findings collectively emphasize that simplified modelling approaches while being efficient, are fundamentally limited in their ability to capture fracture-driven behavior. This limitation becomes particularly problematic in extreme loading scenarios, where connection failure, rather than member yielding, governs global response. The inability to replicate fracture not only affects the prediction of ultimate capacity but also distorts deformation patterns, energy dissipation and failure sequences.

Further evidence of this limitation is provided by [17], who developed a moment-rotation model for a double-span beam under tensile catenary action using a simplified FE approach that excluded explicit beam-to-column connections. By relying solely on the flexural and tensile capacities of beam sections, the model neglected the influence of connection ductility and strength on collapse mechanisms. While such an approach may be acceptable for connections with ample rotational capacity, it risks overestimating nonlinear response and collapse resistance for joints with limited ductility, thereby reducing its general applicability. In contrast, fracture-informed modelling strategies demonstrate substantially improved agreement with experimental observations. Dinu et al. [6] incorporated ductile damage models calibrated through fracture strain and stress triaxiality to match observed breaking points in experiments. Their results showed close correspondence between numerical and experimental load-displacement curves, with peak loads and ultimate displacements accurately captured across specimens. This consistency highlights the capability of fracture-based models to reproduce both global response and local failure phenomena when adequately calibrated.

A comprehensive comparison of simplified and fracture-based approaches was presented by Yang and Tan [1], who examined six connection types subjected to catenary action. Their numerical analyses revealed that explicit dynamic solvers were particularly effective in simulating the full fracture process, including crack initiation, propagation, and complete connection failure. In contrast, static solvers were able to capture initial fracture initiation and partial crack growth but terminated prematurely due to numerical instability caused by excessive cracking. Importantly, simulations conducted without fracture criteria significantly overpredicted load-carrying capacity by approximately 50% relative to experimental results, demonstrating the unconservative nature of neglecting damage evolution. Collectively, the literature reveals a clear dichotomy between simplified and fracture-based finite element modelling strategies.

Simplified approaches offer computational efficiency and ease of implementation but systematically fail to capture-driven behavior, leading to overestimation of strength and ductility under extreme loading. Fracture modelling, while computationally demanding and data-intensive, provides a more reliable representation of connection behavior and failure progression. The challenge for current research lies in balancing modelling fidelity with practical feasibility, particularly in developing calibrated yet computationally efficient frameworks capable of accurately predicting fracture-sensitive connection response. This gap underscores the need for further methodological refinement to improve the robustness and credibility of finite element-based assessments of steel connection performance under extreme conditions.

This study aims to compare the load-resisting performance of double-span steel beams with and without incorporating complex fracture material modeling via element deletion. By analyzing both modeling approaches, the research aims to provide insights that can guide informed decisions in connection design, ensuring structural integrity and safety under various loading scenarios

NUMERICAL ANALYSIS

Validation of Numerical Modelling Technique

This research presents a double-span steel beam obtained for a segment of the perimeter beam, illustrated in Figure 2 [6]. The extracted double-span beam consists of two universal beams (UB) with identical span lengths (L), a column joint placed at the midpoint of the span to simulate the absence of a column, and two universal columns (UC) situated at each end of the span. Both the beam and column fall into the Class 1 category. The validity of the finite element method employed in this study was confirmed by comparing it against experimental findings reported by [6]

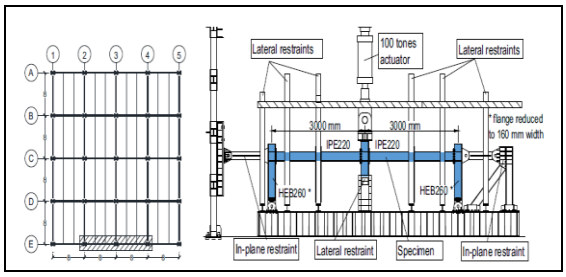

Figure 1. Experimental setup of specimen [6]

A series of incremental Pushdown tests on different moment connections was carried out to evaluate their effectiveness in situations where columns are lost. In the experimental setup, two 3000 mm IPE220 beams were supported by HEB260 columns at both ends of the beam span. The beam-to-column connection utilized by [6] for validation was the welded cover plate flange (CWP) configuration. To model all the parent elements, cover plates, and shear tabs in [6], an S4R shell element was utilized as depicted in Figure 3. The materials characteristics for every structural component within the experimental configuration employed by [6], where ultimate strain and fracture strength were determined through experimental testing of individual material specimens.

Given that the numerical examination conducted in [6] incorporated fracture material modelling, progressive ductile damage criteria were designated within the properties section of the ABAQUS software. To accurately define structural failure or damage within the analysis, the Damage Evolution sub-option was activated within the ductile damage feature. This entailed specifying parameters such as displacement type, linear softening, and maximum degradation. By employing these settings, the analysis ensures a clear delineation of structural failure or damage progression, thereby enhancing the fidelity of the simulation results.

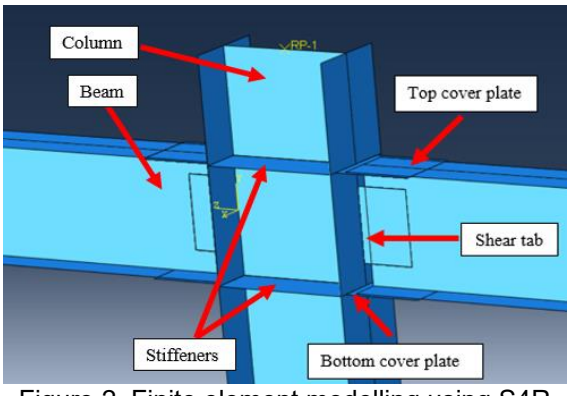

Figure 2. Finite element modelling using S4R shell element

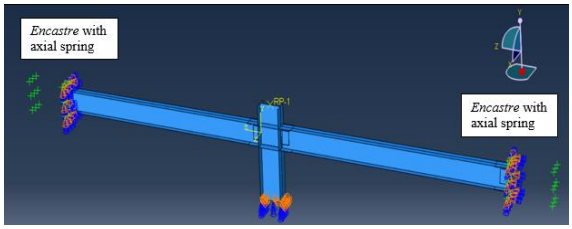

Figure 3. Assembly of finite element modelling

All interactions among the beam-to-column connections were established through tie-constraint interactions to guarantee welding rigidity and force transmission. Reference Point 1 (RP-1) was selected to tie the entire top region of the central column as a rigid body-type interaction, replacing the metal plate utilized in a prior study [6]. The concentrated force was allocated to RP-1.

The boundary conditions for both ends of the supporting column were described as *Encastre*, where all translational and rotational movements were restricted, simulating a fully rigid connection in a real-world scenario (refer to Figure 4). The boundary condition for the central column was depicted with horizontal movement being restrained. In the finite element modelling, axial springs were incorporated at both ends of the column to represent the in-plane restraint observed in the experimental setup depicted in Figure 2. The SPRING element, shown in Figure 4, was chosen with axial stiffness values of 308 kN/m and 95 kN/m for providing robust reaction at the left and right columns, respectively. Upon completion of the development of the finite element model, the subsequent step involves running the analysis, followed by comparing the results obtained with the experiments conducted [6].

Proposed Specimen of Double-Span Steel Beams

The proposed specimen of double-span steel beams in this research was sourced from Subki et al. [21] and is illustrated in Figure 5. This study employed two different finite element modelling methods to simulate the structural failure of the double-span steel beams. The initial approach, indicated as the non-fracture material model, employs a straightforward technique representing the welded beam-to-column connection using tie-constraint interaction with elasto-plastic materials. In this method, the tensioning effect is indicated by the parameter equivalent plastic strain (PEEQ), without considering the impact of the damage evolution model. Conversely, the second approach, referred to as the fracture material model, similarly represents the beam-to-column

connection using tie-constraint interaction. However, in this alternative method, the impact of the damage evolution model is taken into account through the use of the plasticity damage incorporating element deletion method.

In this study, a perfect weld is represented using a tie-constraint interaction, which enforces full compatibility of translational and rotational degrees of freedom between beam and column elements, thereby modelling the weld joint as fully rigid with complete force and moment transfer. This assumption has been adopted by Dinu et al. [6] to investigate global structural response without explicitly modelling weld material properties. Accordingly, explicit weld modelling was not considered as the focus is on comparing non-fracture and fracture models of steel members. Nevertheless, this assumption is acknowledged as a limitation, as neglecting weld behavior may lead to conservative or unconservative predictions and potentially overestimate fracture in the connected members.

The materials utilized in this parametric investigation were adopted in a similar manner to the study conducted in [21]. As depicted in Figure 5, two universal beams of equal length were joined together via a welding connection to a universal column. Horizontal stiffeners were installed at every column to handle the horizontal stress transferring from the beam flange to the column. A pushdown force was applied on top of a metal plate, which was connected to the upper section of the central column. The previous study by Subki et al. [21] analyzed a double-span beam using a modelling technique that did not consider the effect of a damage evolution model.

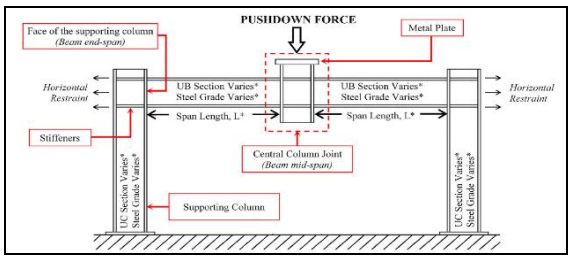

Figure 4. Details of double-span beam specimen [21]

The analysis focused on the behavior of the beam without taking into account the progression of damage over time. This research may be valuable for understanding the structural response of the beam under certain conditions, but it does not account for the impact of damage evolution on its behavior. Therefore, this study will comprehensively analyze and discuss both the non-fracture material model and the fracture material model.

This will involve elucidating the distinctions between these two approaches, from the initial stages of geometric modelling to the analysis of the results obtained. It is crucial to ensure that the fracture material model produces precise damage assessments and outputs. This paper examines three different lengths for analysis, both with and without incorporating the fracture material model, as outlined in Table 1. Sample sizes of 3000 mm, 6000 mm, and 9000 mm were used in this study. The varying numbers were chosen based on prior studies [17, 22, 23] to distinguish their effect on the elastic bending stiffness and tensile catenary action development. The numerical analysis of the specimen was conducted using ABAQUS Standard finite element software, which proved its reliability and accuracy in the previous studies by [6, 17, 21]. Nonlinear static analysis in ABAQUS software is suitable for problems involving large deformations, elastic-material behavior, and changes in physical contact [24].

Finite Element Modelling Technique for Proposed Specimen

Geometrical modelling

The initial stage consisted of developing a detailed three-dimensional geometric model of the double-span welded steel beam-to-column connections. The geometry encompasses the primary materials, such as the Universal Beam (UB) and Universal Column (UC), along with any other pertinent features or components of the joint.

Table 1. Length of specimen

Non-fracture specimen	Fracture specimen	Beam size	Column size	Length span (mm)	Steel grade
NF3000	FR3000	UB533x210x92	UC305x305x198	3000	355
NF6000	FR6000			6000	
NF9000	FR9000			9000	

The geometric components were constructed using the S4R element, which is a 4-node first-order shell element with reduced integration. To form the beam and column sections, a 3D deformable-type shell extrusion was opted for. The supporting columns at the end of each span utilized a base feature of a shell planar to depict the faces of the column flange that are connected to the beam section within the central column joint. A horizontal stiffener was installed between flanges to carry the horizontal stress from the beam flanges. This geometric modelling technique was applied to both the analysis utilizing the non-fracture material model and the analysis utilizing the fracture material model.

Material modelling

For a simulation to be correct, the various components of the model must be assigned to the necessary material properties. Mechanical properties such as yield strength, Modulus of elasticity, and Poisson's ratio must be accurately defined. The stress-strain curve of the hot-rolled steel grade S355 used in the present research is presented in Figure 6. The stress-strain relationship was established by incorporating the method of Holzer et al. [25]. The material model introduced consists of (1), (2), and (3).

$$f = E\varepsilon, \qquad 0 \le \varepsilon \le \varepsilon_y \tag{1}$$

$$f = f_y \varepsilon_y, \qquad \varepsilon_y \le \varepsilon \le \varepsilon_{sh} \tag{2}$$

$$f = f_y \left[1 + \left(\frac{\varepsilon - \varepsilon_{sh}}{\varepsilon_u - \varepsilon_{sh}} \right) \left(\frac{f_u}{f_y} - 1 \right) e^{\left(1 - \left(\frac{\varepsilon - \varepsilon_{sh}}{\varepsilon_u - \varepsilon_{sh}} \right) \right)} \right], \quad \varepsilon_y \le \varepsilon \le \varepsilon_f \tag{3}$$

Where f is the stress, ε is the strain, E is the Young's Modulus, fy is the yield stress, fu is the ultimate stress, εy is the yield strain, εu is the ultimate strain, εsh is the strain hardening, and εf is the fracture strain.

Given that the analysis was centered on the nonlinear static analysis, the ABAQUS program should be configured with an appropriate nonlinear material of elastic and plastic parameters, as outlined in Table 2.

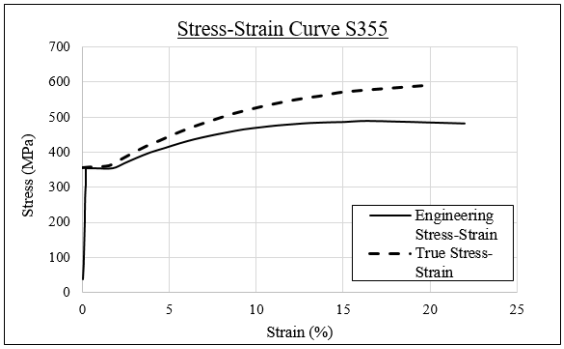

Figure 5. Stress-strain curve of hot-rolled steel grade S355

In implementing the proposed fracture material model to mimic the damage of a steel beam, the progressive damage and failure models which available in the ABAQUS software were employed. The "Damage for ductile metals" feature allows the beam to experience substantial plastic deformation during the necking phase before reaching the fracture point [26]. In order to characterize material degradation, a sub-option for damage evolution was integrated into the ductile damage setting of the material model. This included defining parameters such as displacement type, linear softening, and maximum degradation. Once damage has initiated, the material gradually loses its rigidity in line with the recommended damage evolution response. The model integrates the removal of mesh elements resulting from the tearing of the structure. Progressive damage models facilitate a continuous degradation of material stiffness. The coefficient governing ductile damage and the selection of damage evolution are intricately connected to both mesh size and shape. The specifics of this meshing approach will be outlined in Subsection Mesh modelling technique. To ensure alignment with experimental breaking points, adjustments were performed for each material to account for changes in fracture strain and displacement at failure.

Boundary condition and interaction

The modelling of the double-span steel beam specimen included tie-constraint interaction for all beam-to-column connections, demonstrating the flexural fixity of the components and enabling the transfer of forces within allowable limits.

Table 2. Mechanical properties of S355 hot rolled steel

ρ (kg/m^3)	*E* (MPa)	*v*	f_y (MPa)	f_u (MPa)	ε_y (%)	ε_{sh} (%)	ε_u (%)	ε_f (%)
7850	2.1x10^5	0.3	355	490	0.17	1.70	16.53	22.00

As shown in Figure 7, a concentrated force was exerted on Reference Point 1 (RP-1), which was selected to link all the top regions of the central column using rigid body-type interaction. This is done to make sure that the load is distributed evenly throughout the column section and to keep it from concentrating solely on the column web.

The boundary condition applied to both ends of the supporting columns, referred to as RP-2 and RP-3, were set to *Encastre*. This choice ensures fully rigid connections, effectively preventing any translation or rotational movement within the structure. Such boundary conditions impose constraints on all active structural degrees of freedom within the specified region. In contrast, at the bottom of the central column, designated as RP-4, a YASYMM condition was employed. This setting, where U1=U3=UR2=0, assumes horizontal restraint, allowing only vertical movement.

Analysis procedure and loading scheme

In addressing the nonlinear behavior within this study, the Static-Riks analysis procedure was judiciously chosen. This methodology, renowned within the ABAQUS community for its efficacy, is specifically tailored to confront challenges posed by significant deformations and nonlinear material properties [24]. Its robustness makes it particularly adept at capturing lateral stability nuances and post-buckling behaviors inherent in structures under compression. The Static-Riks method offers a systematic approach to tracing equilibrium paths beyond bifurcation points, crucial for stability analysis. Its utilization extends to a wide array of applications, with notable emphasis on simulating structures subjected to compression, such as shells and columns. By harnessing this technique, engineers can accurately predict the intricate interplay between structural elements, shedding light on critical aspects like load-bearing capacity and structural integrity.

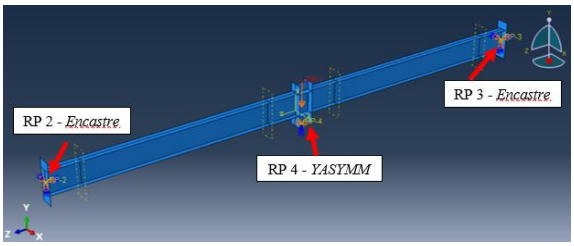

Figure 6. Boundary condition and loading scheme of finite element modelling

During this stage, the basic Nlgeom setting was activated to instruct the ABAQUS software to account for geometric nonlinearity in this phase of analysis and in all subsequent steps. An automatic incrementation method was employed with a maximum of 1000 increments and an initial arc length of 0.01. For the fracture material model analysis, the Status variable in the Field Output Request needed to be defined to ensure proper display of element failures in the results. The analysis was continued until the job was either aborted or terminated by the software. This was done to ensure that the simulation captured the full range of the material's behavior under loading and provided accurate predictions of critical stress or displacement leading to fractures.

Mesh modelling technique

The model has adopted a plastic hinge meshing scheme, chosen for its capacity to effectively replicate the nonlinear behavior of structural elements, potentially resulting in reduced computation time [21]. Hoang et al. [27] also reported that this meshing approach, incorporating plastic hinges, has proven successful in accurately reproducing structural responses under extreme loading conditions. Its application extends in enhancing structural design and improving simulation performance. This method enables the identification of plastic hinges or deformations along the length of the member, offering an efficient means to assess the behavior and cost of beam-to-column connections. Consequently, the beam structure was partitioned by creating sections at both ends, as depicted in Figure 8. A finer mesh was applied to Segment 1 (both ends of the beam), while Segment 2 (middle section) used a coarser mesh size. The length of Segment 1 was determined by using (4).

$$L_P = L\left(1 - \frac{1}{S}\right) \tag{4}$$

Where L_p is the plastic hinge length, L is the length of beam span, and S is the shape factor (S=1.14 for a universal beam).

It was anticipated that as the sectional yielding progressed with additional bending of the beam, the plastic hinge length would increase. In this study, it was proposed that the suggested segment length (L_S) be twice the theoretical plastic hinge length. Furthermore, for the fracture material model analysis, an extra element control must be specified in the Element-Type option. It is imperative to integrate element deletion into the simulation process to represent the initiation and progression of cracks in structural elements.

This involves removing elements from the finite element model as the crack propagates, thereby facilitating a precise depiction of structural failure. The fraction strain employed in the ductile damage material model was calibrated based on methodologies previously validated in the literature. Following the approaches adopted by Dinu et al [6] and Gao [7], the fracture strain parameter was selected by correlating numerical predictions with experimentally observed fracture initiation and global load-displacement behavior. The chosen fracture strain ensures that element deletion initiates at locations consistent with reported experimental failure modes and near the peak load level of the reference tests. This calibration procedure provides a balance between numerical stability and physical realism, enabling accurate representation of fracture initiation and progression in steel members.

A formal mesh sensitivity study was not included in this study. Instead, the adopted mesh configuration was selected based on prior validation through both experimental and numerical investigation reported in [6][21]. The meshing strategy follows that used in previous studies, where numerical models were rigorously validated against experimental results demonstrating mesh adequacy for capturing global response and fracture behavior. To ensure reliability, the numerical results obtained in this study were directly compared with corresponding experimental and numerical findings from the reference study [6], showing close agreement in terms of load-displacement response and failure mode. This consistency indicates that the selected mesh density is sufficient for the objectives of the present analysis. Nevertheless, the absence of a dedicated mesh sensitivity analysis is acknowledged as a limitation, and future work may include systematic mesh refinement to further assess numerical convergence.

It is crucial to acknowledge that the use of damage plasticity features in ABAQUS software requires advanced skill and knowledge. The choice of damage initiation and damage evolution law is significant, as the parameters of each element must be appointed correctly to ensure the results are accurate and reliable. Incorporating element deletion methods necessitates specifying the maximum degradation for each element in the damage plasticity section, which affects the removal of damaged elements during the simulation process.

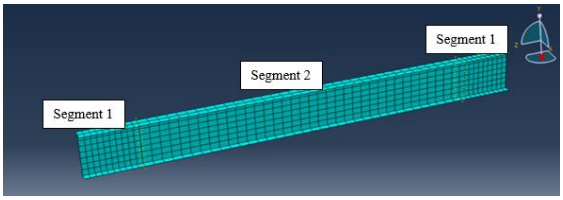

Figure 7. Plastic hinge meshing scheme

While Static-Riks analysis is recognized for its applicability in examining nonlinear static stress/ displacement analysis, particularly for problems with potential buckling behavior, it still has inherent limitations in this study. The minimum and maximum values of arc length incrementation must be specified correctly, as they affect stability and convergence towards a correct equilibrium configuration. Excessively large arc length increments can cause convergence issues, whereas excessively small increments can prolong the convergence time. The limitations in time incrementation set up by the ABAQUS software might cause analysis termination to occur. Combining the use of plasticity damage and element deletion methods with nonlinear Static-Riks analysis in ABAQUS software increases the complexity of the analysis. This necessitates additional computational resources and expertise to manage the sophisticated modelling and ensure accurate results.

RESULTS AND DISCUSSION

Validation Results

Before advancing with the study, it is essential to validate the pushdown force results against [6] to ensure accuracy. As depicted in the graph presented in Figure 9, both the numerical models for non-fracture and fracture analysis were successfully validated against the pushdown test results [6]. The experimental result reported that the welded cover plate flange connection (CWP) can reach the maximum applied load up to 603 kN with a vertical displacement of 519 mm. As can be seen in Figure 9, the load-displacement curves from finite element analysis of this study match well with the peak loads and ultimate displacements of the experimental results and finite element analysis in [6].

Figure 10 depicts the extended line of the Finite Element Analysis (FEA) Non-Fracture from this study, illustrating the maximum force and displacement before a decrease in force occurs. It was observed that, by omitting plasticity damage and element deletion methods, the ultimate force and displacement were higher compared to specimens incorporating these features. The decrease in strength capacity and

ultimate displacement was estimated to be around 50% each. However, a notable disparity between this research and the prior study lies in the observation of the tearing zone, as delineated in Figure 11. In the case of the CWP connection (Figure 11(b)), failure initiation occurs when the bottom plate fractures under tension near the weld with the column.

Subsequently, the fracture propagates through the shear tab, ultimately resulting in the complete detachment of the beam from the columns. It is worth noting that the fracture initiation zone in this study (Figure 11(a)) differs from that of the earlier paper, as it occurred at the weakest point of the plastic hinge. In this study, the modelling of bolts has been disregarded and excluded from the geometric modelling and analysis procedure due to time constraints. Both sets of results were compared to another study, as depicted in Figure 12 [13]. Figure 12(a) and (b) respectively illustrate the tearing zone for fully welded connections and bolted connections. The tearing zone in Figure 11(a) is observed to be similar to that of Figure 12(a), occurring at the weakest point of the beam element's plastic hinge. Conversely, the tearing zone for bolted connections, as shown in Figure 11(b) and Figure 12(b), is seen to fail along the line of the bolts.

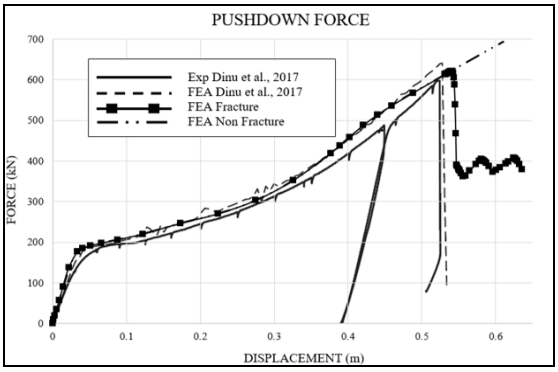

Figure 8. Validation of pushdown force result

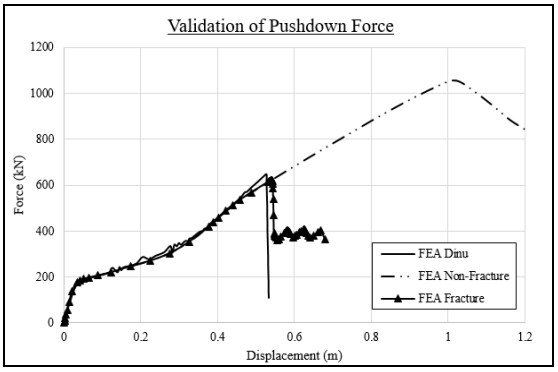

Figure 9. Extended graph line of FEA Non-Fracture

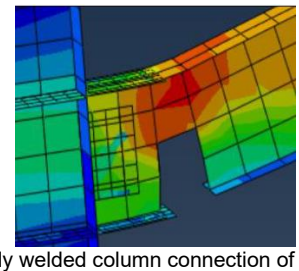

(a) Fully welded column connection of this study

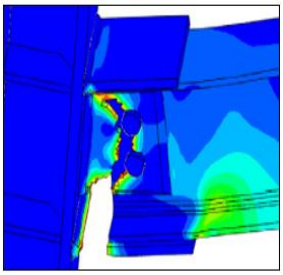

(b) CWP connection [6]

Figure 10. Tearing zone

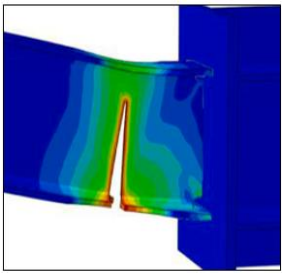

(a) Fully welded connection

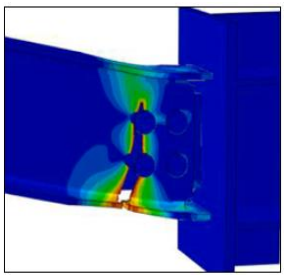

(b) Bolted connection

Figure 11. Tearing zone [13]

Load-Resisting Mechanisms

Load-displacement curve

The load-displacement curves depicted in Figure 13 to Figure 15 illustrate the behavior of specimens labelled as L3000, L6000, and L9000, respectively. Initially, during the loading phase, both non-fracture and fracture material models displayed elastic characteristics across all specimens. As the load was applied, there was a nearly linear increase in load due to the inherent stiffness of the connection, without any observable collapse or weakening of the connection's components as aligned with the standard basis for steel joint design in Eurocode 3 Part 1-8: Design of joints [28][29]. Notably, both

non-fracture and fracture specimen exhibited similar yielding points and displacements at the central column, approximately at 1236 kN and 25 mm, respectively. This indicates a comparable response despite the presence of fractures in the material.

As shown in Figure 13, the points at which yielding occurs differ slightly between the non-fracture and fracture conditions, measuring 1236 kN and 1238.2 kN, respectively. The associated displacements are 25.7 mm and 27.0 mm for non-fracture and fracture cases, respectively. In the non-fracture scenario, the applied forces continue to rise steadily until reaching the ultimate strength, which peaks at 3883.2 kN, coinciding with an ultimate displacement of 1480.4 mm. Conversely, in specimens considering the fracture material model, the ultimate strength begins to diminish at a force equivalent to 2122.1 kN accompanied by a displacement at the central column of 573.4 mm. This observation underscores the distinct behavior influenced by the presence of fractures within the material.

The load-displacement curve depicted for specimen L6000 in Figure 14 reveals a yielding point of approximately 619.5 kN, coinciding with a displacement of 92.5 mm. In the case of the non-fracture material model, the applied forces steadily increase until they reach the ultimate strength, peaking at 3216.1 kN, with an ultimate displacement of 2282.5 mm. Conversely, when considering the fracture material model, the ultimate strength begins to decline at a force equivalent to 2218.9 kN, accompanied by a displacement at the central column of 1365.9 mm. This demonstrates a notable deviation in behavior depending on whether fractures are taken into account within the material model.

The yielding force and displacement for specimen L9000 can be determined by analyzing the data presented in Figure 15. Both the non-fracture (NF9000) and fracture (FR9000) material models exhibit a yielding force of 406 kN and a yield displacement of 152.7 mm. The NF9000 specimen reaches its peak load at 2717.3 kN, occurring at a displacement of 2919.9 mm, before gradually decreasing. The fracture specimen, FR9000 experiences a decline in strength capacity after reaching an applied load of 2129.3 kN, with a displacement of 2050.4 mm. This distinction in behavior highlights the influence of material integrity on the load-displacement characteristics of the specimen. In all three fracture specimens, the onset of fracture-induced failure resulted in early stiffness degradation and a reduced peak load capacity, which is consistent with trends reported in the literature [26, 29, 30].

The contour plot of the equivalent plastic strain (PEEQ) in Figures 16(a), (c) and (e), indicate that the beam tension flange exceeds its fracture strain, causing a reduction in load-bearing capacity, in agreement with numerical studies [31][32] that reported crack initiation and strength degradation associated with high PEEQ concentrations at weld-beam interfaces. Numerical analysis of all non-fracture specimens consistently showed significant stress build-up in the beam vicinity near the welding connection with the column. This finding underscores the critical role of stress distribution and material behavior in determining structural integrity under load.

Figure 16(b), (d) and (f), depict the initial failure stage, characterized by tension-induced fracturing at the bottom flange of the beam near its welding connection with the column. This fracture initiates and subsequently propagates into the beam's web, ultimately resulting in the complete detachment of the beam from the column.

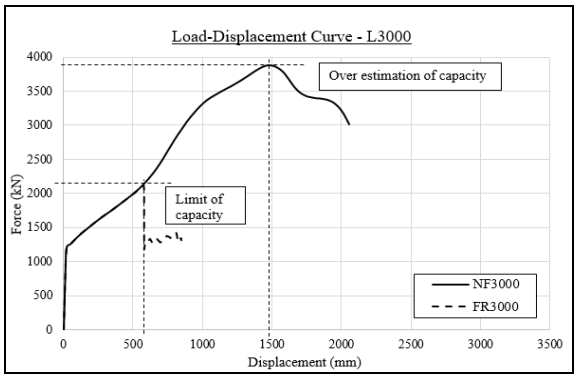

Figure 12. Load-displacement curve for specimen L3000

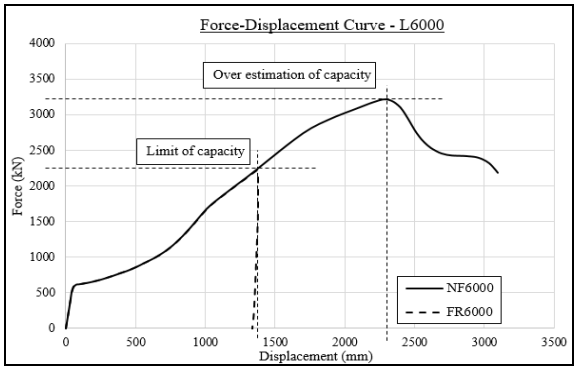

Figure 13. Load-displacement curve for specimen L6000

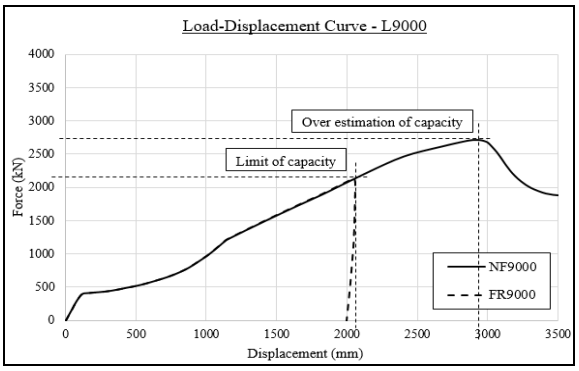

Figure 14. Load-displacement curve for specimen L9000

Upon examining the load-displacement curves plotted in Figure 14 to Figure 16, it becomes apparent that there is an overestimation of the bearing capacity and ultimate displacement when considering non-fracture specimens. These overestimation values have been quantified and organized in Table 3. In many finite element designs, there exists a discrepancy between the idealized conditions assumed and the actual conditions observed in real-world scenarios, such as the fracture of the specimen. Consequently, it is imperative to consider a reduction factor in strength capacity calculations when designing structures to account for potential collapses, particularly in simplified numerical simulations. This underscores the importance of accounting for realistic material behavior and failure mechanisms in structural design processes.

Nonetheless, the reduction factor proposed in this study is constrained by its failure to incorporate the welding strength of real-world conditions, including mechanical properties and welding craftsmanship. The analysis proceeded under the assumption that the welding connection possessed significant stiffness and ductility. However, in a more comprehensive modelling of weld or bolt connections, the resulting reduction in strength capacity may either increase or decrease.

This emphasizes the importance of accurately representing the properties and behavior of welding or bolting in structural analyses to ensure more realistic predictions of strength capacity. Incorporating such details can lead to more reliable assessments of structural integrity and performance under various loading conditions.

Moment-rotation response

The moment-rotational response curve will utilize data on the moment to plastic moment ratio (M/Mp) and rotation to yield rotation ratio (θ/θy). The plastic moment (Mp), chord rotation (θ), and yield rotation (θy) can be determined using equations (5), (6), and (7), respectively. The moment data resulting from the pushdown force and the displacement at the central column will be directly obtained from the ABAQUS software.

$$M_p = W_{pl} f_y \tag{5}$$

$$\theta = \frac{\Delta}{L} \tag{6}$$

$$\theta_y = \frac{W_{pl} f_y L}{6 E I_b} \tag{7}$$

Where, W_{pl} is the plastic section modulus, f_y is the material yield stress, Δ is the vertical displacement at central column, L is the length of the beam span, I_b is the second moment of area of the beam.

The moment-rotation response for specimens L3000, L6000, and L9000 are depicted in Figures 17 to Figure 19, respectively. These curves were generated using the calculated mechanical properties listed in Table 4. Initially, the data extracted from the ABAQUS software was utilized to plot graphs of moment (M) in kNm against chord rotation (θ) in radians.

Table 3. Reduction factor of strength capacity

Specimen	Ultimate strength (kN)	Ultimate displacement (mm)	Reduction in strength capacity	
			Reduction factor	(%)
NF3000	3883.23	1480.48	0.546	54.6
FR3000	2122.12	573.44		
NF6000	3216.19	2282.57	0.690	69.0
FR6000	2218.97	1365.98		
NF9000	2717.35	2919.94	0.783	78.3
FR9000	2129.30	2050.45		

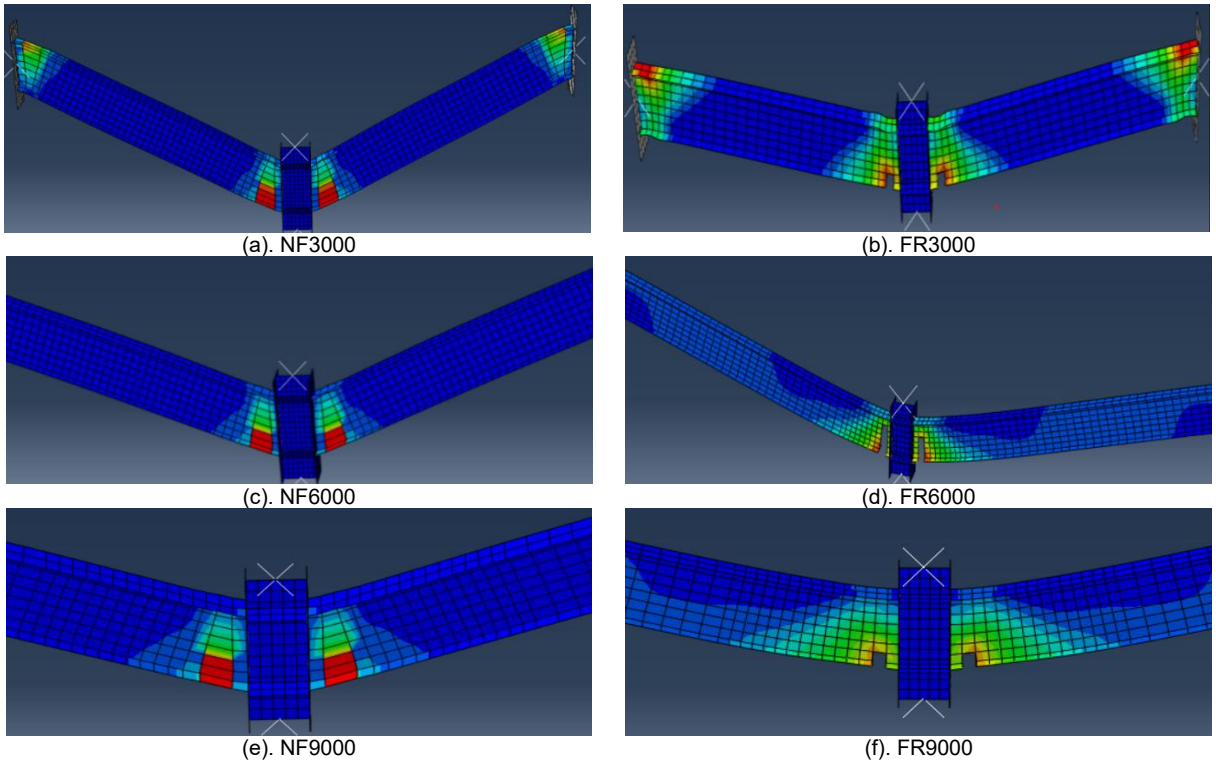

(a). NF3000 (b). FR3000

(c). NF6000 (d). FR6000

(e). NF9000 (f). FR9000

Figure 16. PEEQ contour plot

Subsequently, these raw plots were further processed to generate the normalized moment-rotation response curves, which are discussed in detail in this section. The normalized moment-rotation response curves provide valuable insights into the structural behavior under loading conditions. By normalizing the data, it becomes possible to compare the responses of different specimens more effectively, facilitating a deeper understanding of how various parameters such as material properties and loading conditions influence structural performance.

In Figure 17, it is evident that both the non-fracture and fracture material models have reached their full moment capacities. Specifically, the NF3000 specimen demonstrate a larger rotational capacity, with moment capacity gradually decreasing over time. On the other hand, the FR3000 specimen experiences a significant drop in moment capacity, and its maximum rotation is limited due to beam fracture. This initial decline occurs when the beam reaches its tensile yielding point. However, the beam possesses the capability to regain strength and resist external forces. Consequently, it starts to redevelop its moment capacity until it either reaches the fracture point or experiences the initiation of fracture. The ratio of rotation to yield rotation (θ/θ_y), which is influenced by the displacement at the central column, indicates the beam's capacity to rotate, which becomes constrained once the initiation of beam flange fracture occurs. Notably, when fracture or damage evolution is factored into the analysis, it becomes apparent that the rotation capacity of the non-fracture material model is significantly reduced by more than 60%. This reduction underscores the profound impact that material integrity and the presence of fractures have on the structural behavior, particularly in terms of the beam's ability to deform and rotate under loading conditions.

Similar trends in the relationship between moment to plastic moment (M/M_p) and rotation to yield rotation (θ/θ_y) are evident in Figure 18 for specimen L6000 and Figure 19 for specimen L9000. In both cases, as with specimen L3000, there is a progressive decrease in moment capacity once the beam reaches tensile yielding. However, the specimens exhibit an ability to recover strength, enabling them to withstand applied loads and develop moment capacity once again. In the fracture specimens, namely FR6000 and FR9000, the second decline in moment capacity occurs due to the initiation of fracture at the beam's flange. This pattern emphasizes the critical influence of material integrity on structural behavior, particularly in terms of load-bearing capacity and resilience to deformation. The reduction factor of rotation to yield rotation (θ/θ_y) for all specimens was calculated and documented in Table 5.

Figure 20 illustrates the comparison of moment-rotational responses for all fracture specimens. In terms of moment capacity, all proposed fracture specimens managed to reach their full moment capacities as aligned with Eurocode 3 standards for the Class 1 category [28]. The shorter span specimens exhibited larger plastic deformation before failure. This observation suggests that shorter spans allow for greater deformation before reaching failure. However, a notable difference lies in the ability of the beam to rotate. The shorter beam spans possess larger elastic bending stiffness compared to the longer beam spans, as reported by Subki et al. [17]. This discrepancy results in a delay in the development of tensile catenary action in the shorter spans. The longer spans are more flexible, allowing for earlier initiation of tensile catenary action, which facilitates rotation. Conversely, the shorter spans, with their higher bending stiffness, experience a delay in this process, which affects their ability to allow for beam rotation. This finding emphasizes the importance of considering span length and elastic properties in understanding structural behavior and failure mechanisms.

Tensile catenary action

When subjected to gravity loading, a steel beam primarily experiences the combined effects of shear force and bending moment, with minimal axial force.

Table 4. Calculated mechanical properties

Specimen	Plastic Moment, M_P (kNm)	Yield Rotation, θ_y (rad)	Yield Axial Force, N_y (kN)
NF3000	837.8	0.0036	4153.5
FR3000			
NF6000	837.8	0.0072	4153.5
FR6000			
NF9000	837.8	0.0108	4153.5
FR9000			

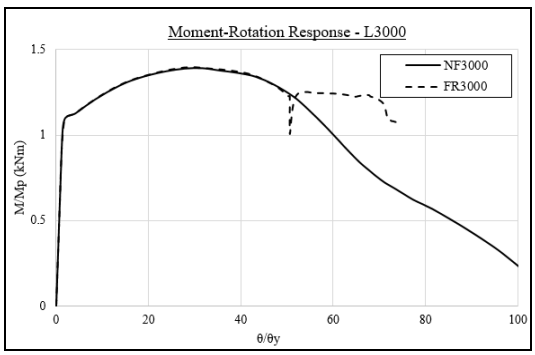

Figure 15.Moment-rotational response of specimen L3000

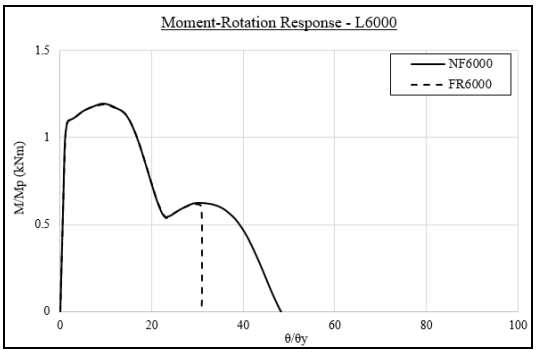

Figure 16. Moment-rotational response of specimen L6000

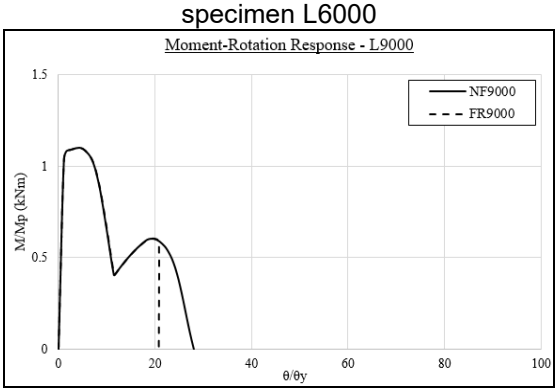

Figure 17. Moment-rotational response of specimen L9000

Table 5. Reduction factor of rotation capacity

Specimen	θ/θ_y	Reduction in rotation capacity	
		Reduction factor	(%)
NF3000	109.0	0.679	67.9
FR3000	74.1		
NF6000	47.5	0.648	64.8
FR6000	30.8		
NF9000	27.6	0.750	75.0
FR9000	20.7		

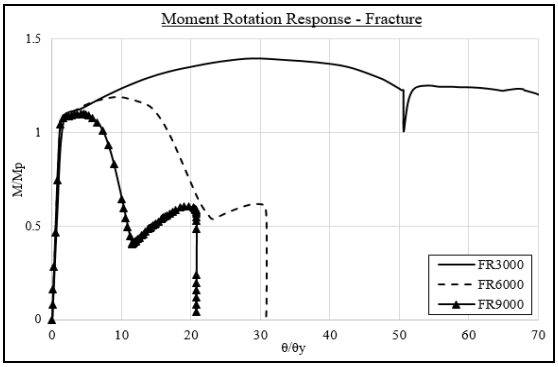

Figure 18. Parametric analysis on the moment-rotational response of the fracture specimen

However, in the event of column loss, the bending moment increases significantly at both ends and the mid-span of the beam, leading to considerable deflection and the formation of

plastic hinges at specific points. Consequently, the beam undergoes axial force. To analyze this behavior, a tensile catenary curve was constructed using data on the axial force resulting from the load applied to the central column, along with the yield axial force ratio (N/N_y) and rotation to yield rotation ratio (θ/θ_y). The yield axial force can be determined using Equation (8). The mechanical properties of each specimen for parametric study were calculated and documented in Table 4, incorporating the provided equations.

$$N_y = A_b f_y \quad (8)$$

Given that, A_b is the cross-section area of the beam.

To create the normalized tensile catenary action curves depicted in Figures 21 to Figure 23, graphs were plotted to illustrate the relationship between axial forces, denoted as N in kN, and displacement at the central column, represented as Δ in mm, for each proposed specimen. The axial force values were derived from the horizontal reaction forces exerted by the supporting end column. These curves provide insights into how the axial force changes in response to displacement at the central column, offering a comprehensive view of the tensile catenary action within the structure. Figure 21 presents a comparison regarding the achievement of tensile catenary action. The non-fracture specimen successfully reached the full tensile catenary action mechanism at a ratio of rotation to yield rotation (θ/θ_y) equivalent to 83.6. However, in the fracture material model, the development of tensile catenary action (TCA) was diminished by 43.7%. This reduction in the development of tensile catenary action can be attributed to the initiation and propagation of fractures within the material. Consequently, there is a decrease in the axial force due to the compromised structural integrity caused by the presence of fractures [1][33].

In Figure 22 and Figure 23, it is evident that all specimens of L6000 and L9000 successfully achieved the development of tensile catenary action. However, notable differences emerged between the fracture and non-fracture specimens. Both fracture specimens, named FR6000 and FR9000, failed earlier compared to their non-fracture counterparts. This premature failure can be attributed to the inability of the fracture specimens to sustain tensile catenary action. The sudden drop in axial force observed in these fracture specimens was directly linked to fractures occurring within the beam elements, compromising their structural integrity. A quantitative analysis revealed in Table 6 that the reduction in tensile catenary action sustainability was significant, amounting to 51% for specimens of L6000 and 69% for specimens of L9000. This reduction underscores the detrimental impact of fractures on the ability of the structure to withstand and distribute loads effectively.

When examining the evolution of Tensile Catenary Action (TCA) by adjusting the beam span length, as illustrated in Figure 24, it becomes evident that the delay in TCA development in the FR3000 specimen is closely linked to the stiffness of the material. The shorter span beam struggles to effectively establish TCA due to the flanges surpassing their tensile capacity, leading to fracture strain in the elements. Conversely, the longer span beam exhibits the capability to establish TCA without inducing local buckling failure. Since longer span beams typically experience greater deflection, this results in a concurrent increase in axial forces, facilitating the formation of TCA.

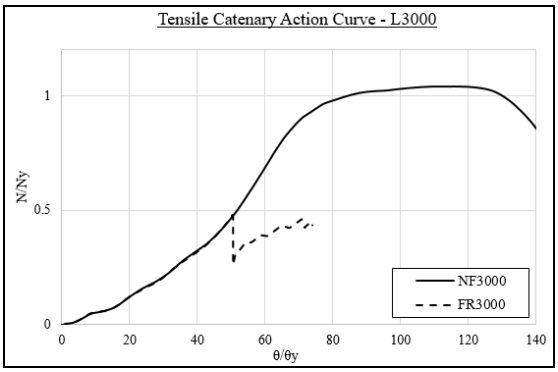

Figure 19. Tensile catenary action curve for specimen L3000

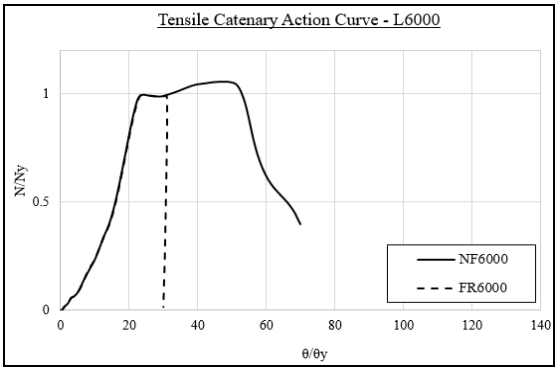

Figure 20. Tensile catenary action curve for specimen L6000

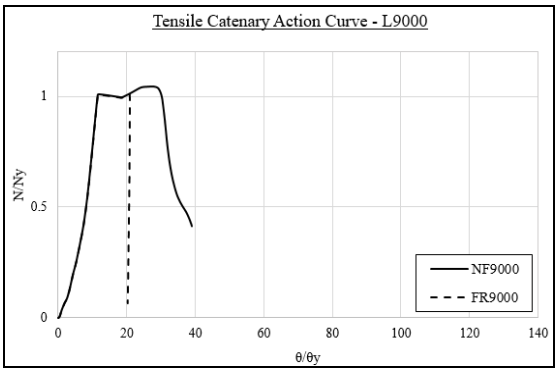

Figure 21. Tensile catenary action curve for specimen L9000

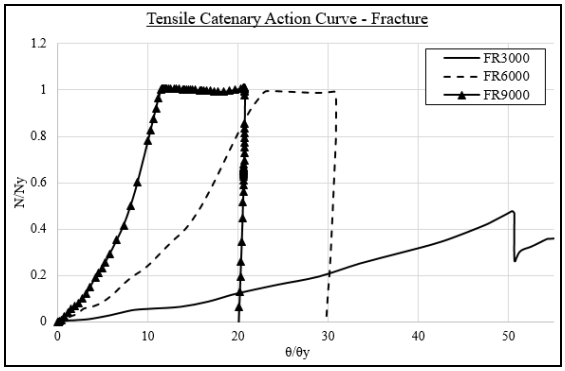

Figure 22. Parametric analysis on tensile catenary action for fracture specimen

Table 6. Reduction factor of TCA sustainability

Specimen	θ/θ_y	Reduction in TCA sustainability	
		Reduction factor	(%)
NF3000	115.4	0.437	43.7
FR3000	50.4		
NF6000	47.6	0.512	51.2
FR6000	24.4		
NF9000	30.0	0.690	69.0
FR9000	20.7		

The analysis results summarized in Table 3, 5 and 6, highlight significant reductions in the capacity of fracture specimens when considering ductile damage and element deletion, with reductions of approximately half compared to models that do not account for these factors. Fracture specimens typically exhibit lower ultimate strength when reaching ultimate deformation. A Finite Element Model (FEM) incorporating ductile damage and element deletion may demonstrate lower loads compared to one without these features.

Incorporating Material Damage, such as Ductile Damage models, involves accounting for the gradual accumulation of damage within a material as it undergoes plastic deformation. The accumulation of damage weakens the material over time, diminishing its ability to withstand loads. By introducing ductile damage into the model, it reflects the realistic behavior of materials, particularly metals, which often experience damage prior to ultimate failure. This inclusion allows for a more precise prediction of the material's response to various loading conditions, enhancing the model's accuracy and reliability.

It is essential to include the element deletion in structural simulations to accurately model local failures or damages. When specific thresholds like stress, strain, or damage levels are surpassed, elements within the model are removed to signify localized failures. This deletion process can be observed in Figures 16 (b), (d) and (f), where elements are automatically eliminated from the model. This typically occurs when a beam reaches its ultimate strength and begins to lose structural integrity before reaching its fracture point, as determined by data analysis.

Meanwhile, the force exerted by non-fractured material models continues to escalate since there are no designated breaking points defined for them. This means that as the damaged areas are represented by the removal of elements, the unaffected material experiences increased stress without an associated failure point. This phenomenon is highlighted in Tables 3, 5 and 6, where the removal of elements in damaged zones contributes to an overall reduction in the structure's load-carrying capacity. This observation underscores the reality that localized damages can significantly weaken a structure, ultimately diminishing its ability to bear loads.

By integrating both ductile damage and element deletion, the Finite Element Method (FEM) offers a more authentic representation of how structures respond to various loading conditions. This realistic portrayal of damage and failure mechanisms can result in a more cautious estimation of the structure's strength when compared to a model that overlooks these factors. In the field of engineering, it is often prudent to design structures with safety margins to ensure their ability to withstand unforeseen loading conditions or uncertainties. The incorporation of ductile damage and element deletion in the FEM can contribute to a more conservative prediction of the structure's load-carrying capacity, aligning with the safety-first approach in engineering design. It is worth noting that the specific impact on the predicted loads relies on the intricacies of the modelling parameters, the accuracy of the chosen damage model, and the appropriateness of the criteria for element deletion. The objective of incorporating

these features is to enhance the accuracy of the simulation by capturing the realistic behavior of materials and structures under loading conditions.

In examining the absence of ductile damage and element deletion models in a Finite Element Model (FEM), it is essential to recognize the potential for downplaying structural weaknesses and load-bearing capabilities. The fracture model utilized in this study is crafted to replicate the gradual build-up of damage within materials and the localized breakdown within a structure, thus offering a more realistic portrayal of its reaction to different loading conditions. As evidenced by the analysis outcomes detailed in above sections, employing an FEM without these crucial models may lead to underestimating the structural requirements and jeopardizing the precision of predicting failures. Nevertheless, it's important to acknowledge that integrating ductile damage and element deletion models requires significant computational resources and a high level of expertise. These techniques often entail intricate algorithms and numerical simulations, demanding skilled practitioners for their effective implementation.

Given the considerable computational resources and expertise needed, it becomes necessary to propose a corrective measure to address the absence of these models. In this study, it is conventionally suggested that designers and researchers consider the use of correction factors. The recommended approach involves utilizing 0.43 of the maximum load/displacement obtained during the analysis. This correction factor is established through meticulous calibration and validation against experimental data, ensuring that the predictions made by the Finite Element Model (FEM) closely align with the actual behavior of materials and structures under various loading conditions. While recognizing the challenges posed by the computational demands and expertise required, the incorporation of correction factors becomes a valuable step in improving the predictive accuracy of FEMs and, consequently, the reliability of structural analyses. This approach helps compensate for the absence of detailed models such as ductile damage and element deletion, allowing for more accurate predictions despite their omission. By carefully adjusting the model outputs using these correction factors, designers and researchers can better account for the complexities of real-world structural behavior.

Furthermore, the recommendation to use a correction factor of 0.43 is not arbitrary; it is the result of rigorous testing and validation against experimental data. This ensures that the correction factor reflects the real behavior of the materials and structures being studied. By basing the correction factor on empirical evidence, it adds a level of reliability to the FEM predictions, even in the absence of more sophisticated models. In essence, while acknowledging the limitations of the FEM due to computational constraints and expertise requirements, the proposal to incorporate correction factors offers a practical solution to enhance the accuracy and reliability of structural analyses. It allows designers and researchers to make more informed decisions based on FEM results, bridging the gap between computational capabilities and real-world complexities.

CONCLUSION

This study demonstrates that neglecting fracture and damage evolution in finite element modelling leads to systematic overestimation of both strength and deformation capacity of double-span steel beams subjected to tensile catenary action. The comparison between non-fracture and fracture models shows that the predicted ultimate strength is reduced by 54.6-78.3%, while rotation capacity is reduced by 64.8-75.0% when fractured behavior is explicitly considered. More critically, the sustainability of tensile catenary action is reduced by 43.7-69.0%, indicating that simplified models substantially overpredict post-yield robustness and collapse resistance. Based on consistent trends across all specimens, a correction factor of approximately 0.43 applied to the maximum load or displacement obtained from simplified non-fracture finite element analysis is proposed. This factor represents the lower bound of observed reductions and provides a conservative yet practical adjustment to compensate for the absence of fracture modelling.

The potential consequences of these findings extend to the fields of structural engineering and numerical analysis. Enhancing the accuracy and reliability of numerical analysis in predicting load-resisting mechanisms and nonlinear behavior of steel beams can significantly improve the design and safety of structural systems. Moreover, the research emphasis on advanced material models and FEM approaches holds promise for shaping the development of more effective and comprehensive simulation techniques in structural engineering. Overall, it has the potential to advance understanding of structural failure and contribute to the evolution of more resilient design and analysis methodologies within the field of structural engineering.

IMPLICATION AND RECOMMENDATION

The research focuses on simulating material failure in real-world scenarios, enabling engineers to anticipate potential failure points and performance under extreme loading conditions. By using plasticity damage and element deletion methods, finite element analysis (FEA) provides a cost-effective and time-saving alternative to experimental tests, offering accurate representations of structural behavior in terms of deformation and fracture. The study also explores the impact of tensile catenary action on structures, providing valuable insights for structural engineering and construction industries. This understanding helps in designing robust and resilient buildings capable of withstanding abnormal loading conditions. Incorporating fracture material model analysis is vital for predicting failure mechanisms and identifying critical points, thus improving design, construction, and maintenance practices for enhanced durability and safety. Comparing cases with and without fracture material model consideration underscores the importance of accounting for fracture behavior in structural performance assessments. This knowledge can influence industry standards, design codes, and practices. Overall, the research contributes to the advancement of finite element analysis techniques, demonstrating their applicability in understanding complex structural behavior.

In finite element analysis, conservative and imperfection models are commonly used to examine double-span beams under column loss scenarios, usually excluding the fracture material model. This study incorporates progressive damage ductile material but assumes a strong welding connection, without considering welding mechanical properties or external factors like weather and workmanship. Future research should integrate the mechanical properties of connections, such as weld and bolt tension, to accurately simulate strength reduction.

The field of structural engineering is constantly advancing in the pursuit of safer and more efficient structures. The findings and limitations of this study highlight the opportunities for future research. Exploring how different geometries, materials, and loading conditions impact the load-resisting mechanisms of welded beam-column connections can provide a more understanding of structural behavior, enhancing the relevance of current findings. Issues with convergence and premature termination of the analysis suggest a need for a detailed review of the time incrementation setup in ABAQUS software. Optimizing this setup could resolve convergence challenges, improving the stability and efficiency of the analysis process. This optimization aims to deliver precise and reliable results while reducing computational

ACKNOWLEDGMENT

The authors would like to thank Universiti Teknologi MARA (UiTM) Shah Alam for their financial support under the *Geran Intensif Penyeliaan* with Grant No: 600-RMC/GIP 5/3 (062/2023).

REFERENCES

[1] B. Yang and K.H. Tan, “Numerical analysis of steel beam-column joints subjected to catenary action” *Journal of Constructional Steel Research*, vol. 70, pp. 1-11, Mar. 2012, doi: 10.1016/j.jcsr.2011.10.007.

[2] B. Yang and K. H. Tan, “Experimental tests of different types of bolted steel beam-column joints under a central-column-removal scenario,” *Engineering Structures*, vol. 54, pp. 112-130, Sep. 2013, doi: 10.1016/j.engstruct.2013.03.037

[3] F. Xie, W. Liu, B. Gu, and H. Qian, “Study on the component-based model of an all-welded beam-column connection for progressive collapse analysis,” *Advances in Civil Engineering*, vol. 2020, pp. 1-11, Nov. 2020, doi: 10.1155/2020/8847866

[4] F. Wang, J. Yang, and Z. Pan, “Progressive collapse behavior of steel framed substructures with various beam-column connections,” *Engineering Failure Analysis*, vol. 109, p. 104399, January 2020, doi: 10.1016/j.engfailanal.2020.104399

[5] P. Stylianidis and J. Bellos, “Survey on the role of beam-column connection in the progressive collapse resistance of steel frame buildings,” *Buildings*, vol. 13, no. 7, p. 1696, July 2023, doi: 10.3390/buildings13071696

[6] F. Dinu, I. Marginean, and D. Dubina, “Experimental testing and numerical modelling of steel moment-frame connections under column loss,” *Engineering Structures*, vol. 151, pp. 861-878, Nov. 2017, doi: 10.1016/j.engstruct.2017.08.068

[7] S. Gao, “Nonlinear finite element failure analysis of bolted steel-concrete composite frame under column-loss,” *Journal of Constructional Steel Research*, vol. 155, pp. 62-76, Apr. 2019, doi: 10.1016/j.jcsr.2018.12.020

[8] J. Ye, G. Quan, X. Yun, x. Guo, and J. Chen, “An improved and robust finite element model for simulation of thin-walled steel bolted connections,” *Engineering*

Structures, vol. 250, p. 113368, Jan. 2022, doi: 10.1016/j.engstruct.2021.113368

[9] M. S. Sulaiman et al., "Simulation and experimental study on distortion of butt and T-joints using WELD PLANNER," *Journal of Mechanical Science and Technology*, vol. 25, no. 10, pp. 2641-2646, Oct. 2011, doi: 10.1007/s12206-011-0701-8

[10] Q. Zhao et al., "Morphological characterization and failure analysis of the ultrasonic welded single-lap joints," *Polymers*, vol. 15, no. 17, pp. 3555-3555, Aug. 2023, doi: 10.3390/polym15173555

[11] A. Anca, A. Cardona, J. Risso, and V. D. Fachinotti, "Finite element modeling of welding processes," *Applied Mathematical Modelling*, vol. 35, no. 2, pp. 688-707, Feb. 2011, doi: 10.1016/j.apm.2010.07.026

[12] B. Sutherland, "Analysis of bolted beam-column connections with multiple bolts analysis of bolted beam-column connections with multiple bolts per row and column web stiffeners per row and column web stiffeners," *Civil Engineering Common*, 2016, Available: https://scholarworks.uark.edu/cgi/viewcontent.cgi?article=1027&context=cveguht

[13] C. Chen, Q. Huang, J. Wang, and C. Yu, "Progressive collapse behavior of joints in steel moment frames involving reduced beam section," *Engineering Structures*, vol. 225, pp. 111297-111297, Dec. 2020, doi: 10.1016/j.engstruct.2020.111297

[14] G. Nadeem, N. A. Safiee, N. Abu Bakar, I. Abd Karim, and N. A. Mohd Nasir, "Evaluation of slip behavior of self-locking modular steel connection," *Journal of Constructional Steel Research*, vol. 197, pp. 107467-107467, Oct. 2022, doi: 10.1016/j.jcsr.2022.107467

[15] X. H. Dai, Y. C. Wang, and C. G. Bailey, "Numerical modelling of structural fire behavior of restrained steel beam-column assemblies using typical joint types." *Engineering Structures*, vol. 32, no. 8, pp. 2337-2351, Aug. 2010, doi: 10.1016/j.engstruct.2010.04.009

[16] F. Liao, W. Wang, and Y. Chen, "Parameter calibrations and application of micromechanical fracture models of structural steel," *Structural Engineering and Mechanics/ Structural Engineering and Mechanics*, vol. 42, no. 2, pp. 153-174, Apr. 2012, doi: 10.12989/sem.2012.42.2.153

[17] N. E. A. Subki, H. Mansor, Y. Sahol Hamid, and G. A. R. Parke, "The development of a moment-rotation model for progressive collapse analysis under the influence of tensile catenary action," *Journal of Constructional Steel Research*, vol. 187, p. 106960, Dec. 2021, doi: 10.1016/j.jcsr.2021.106960

[18] F. Sadek, J. A. Main, H. S. Lew, and S.El-Tawil, "Performance of steel moment connections under a column removal scenario. II, Analysis," *Journal of Structural Engineering*, vol.139, no. 1, pp. 108-119, Jan. 2013, doi: 10.1061/(asce)st.1943-541x.0000617

[19] V. V. Saykin, T. V. Nguyen, J. F. Hajjar, D. Deniz, and J. Song, "Material characterization using finite element deletion strategies for collapse modeling of steel tructures," *Engineering Structures*, vol. 147, pp. 125-133, Sep. 2017, doi:. 10.1016/j.engstruct.2017.05.059

[20] Z. Alomar, L. Maccioni, and Franco Concli, "Development and implementation of element deletion algorithm into an open-source software based on the fracture locus of materials," *Materials (Basel)*, vol. 16, no. 1, pp. 187-187, Dec. 2022, doi:. 10.3390/ma16010187

[21] N. E. A. Subki, H. Mansor, Y. Sahol Hamid, and G. A. R. Parke, "Finite element dynamic analysis of double-span steel beam under an instantaneous loss of support," In *Proceedings of the 5th International Conference on Sustainable Civil Engineering Structures and Construction Materials*, Jan. 2022, pp. 593-610, doi: 10.1007/978-981-16-7924-7_39

[22] P. Stylianidis and D. Nethercot, "Considerations for robustness in the design of steel and composite frame structures," *Structural Engineering International*, vol. 27, no. 2, pp. 263-280, May 2017, doi: 10.2749/101686617x17881932436212

[23] I. Faridmehr and M. Hajmohammadian Baghban, "An overview of progressive collapse behavior of steel beam-to-column connections," *Applied Sciences*, col. 10, no. 17, p. 6003, Aug. 2020, doi: 10.3390/app10176003

[24] "Abaqus analysis user's guide (6.14)," *149.89.49.2021.*

[25] S. M. Holzer, R. J. Melosh, R. M. Barker, and A. E. Somers, "SINGER: A computer code for general analysis of two-dimensional reinforced concrete structures," vol. 1. Solution process," May 1975.

[26] "About progressive damage and failure," *docs.software.vt.edu.*

[27] V.-L. Hoang, H. Nguyen Dang, J.-P. Jaspart, and J.-F. Demonceau, "An overview of the plastic-hinge analysis of 3D steel frames,"

Asia Pacific Journal on Computational Engineering, vol. 2, no. 1, Dec. 2015, doi: 10.1186/s40540-015-0016-9

[28] Eurocode 3: Design of steel structures – Part 1-8: Design of joints, EN 1993-1-8:2005, European Committee for Standardization (CEN), Brussels, Belgium, 2005.

[29] S. N. R. Shah, N. H. R. Sulong, M. Shariati, and M. Z. Jumaat, "Steel rack connections: identification of most influential factors and a comparison of stiffness design methods," *PLoS ONE*, vol. 10, no. 10, p. e0139422, Oct. 2015, doi: 10.1371/journal.pone.0139422

[30] Z. Tang, X. Yang, H. Liu, and H. Xue, "Numerical simulation with an improved ductile fracture model for steel connections considering effect of element size," *Journal of Constructional Steel Research*, vol. 223, p. 109031, Sep. 2024, doi: 10.1016/j.jcsr.2024.109031

[31] M. A. Shaheen, K. D. Tsavdaridis, and S. Yamada, "Comprehensive FE Study of the hysteretic behavior of Steel–Concrete Composite and Noncomposite RWS Beam-to-Column connections," *Journal of Structural Engineering*, vol. 144, no. 9, Jun. 2018, doi: 10.1061/(asce)st.1943-541x.0002124

[32] S. Naimi, M. Celikag, and A. A. Hedayat, "Ductility enhancement of Post-Northridge connections by multilongitudinal voids in the beam web," *The Scientific World JOURNAL*, vol. 2013, no. 1, p. 515936, Jan. 2013, doi: 10.1155/2013/515936

[33] O. A. Harry and Y. Lu, "Simplified theoretical model for prediction of catenary action incorporating strength degradation in axially restrained beams," *Engineering Structures*, vol. 191, pp. 219–228, Apr. 2019, doi: 10.1016/j.engstruct.2019.04.043